15

Estimating atmospheric transparency during darkness based on data from all-sky cameras with a narrow spectral range

© A.B. Beletsky, M.A. Taschilin, I.P. Yakovleva, E.V. Devyatova, S.V. Podlesny, R.V. Vasiliev, A.V. Tatarnikov, V.P. Lebedev

Institute of solar-terrestrial physics of Siberian branch of Russian academy of sciences, Irkutsk, Russia
e-mail: miketash@iszf.irk.ru

Received October 13, 2025
Revised November 5, 2025
Accepted November 10, 2025

This paper presents a methodology for assessing the transparency of the Earth's atmosphere at night using all-sky imagers with a narrow spectral range, designed to record the spatial distribution of the intensity of emissions from the Earth's upper atmosphere. The imagers operate in monitoring mode at the Geophysical Observatory of the Institute of Solar-Terrestrial Physics (Tory, Buryatia, 51°48′N, 103°04′E). The developed methodology is currently being used to address a number of problems, including: assessing atmospheric transparency at night; relative calibration of all-sky imagers using „reference"clear nights; obtaining additional information for interpreting data on the spatial distribution of atmospheric emission intensity and evaluating criteria for identifying traveling wave disturbances. In the future, it is planned to improve this method by optimizing the calculation algorithm, using more modern star catalogs, and verifying the absolute calibration of the all-sky imagers used.

Keywords: atmospheric emissions, atmospheric extinction, all-sky imagers, Aeronet, atmospheric transparency.

DOI: 10.61011/TP.2026.03.63173.288-25

Introduction

Aerosol particles present at various atmospheric altitudes affect the spectral distribution of twilight and night airglow. The study of self-radiation of the Earth's upper atmosphere and astronomical observations at night time shall consider atmospheric transparency and other astronomical climate and optical weather parameters because airglow intensities measured at various atmospheric transparencies can differ very much from each other [1]. The effect of atmospheric aerosol on ground observations of airglow in atomic oxygen emission lines, [OI] 557.7 and 630.0 nm, was analyzed in [2] using previously obtained spectral characteristics of the aerosol optical depth (AOD) and water content of atmosphere. Dependence of correlation coefficients between 557.7, 630.0 nm and AOD emission intensities is reported and its nonlinear behavior has been identified. In [1,2], these atmospheric transparencies were measure using a sun photometer and generally may not reflect the aerosol behavior at night time. CCD fisheye lens camera were used in some studies to evaluate a set of night sky properties such as atmospheric transparency, night sky brightness, clouds, percentage ratio of clouds, etc. For example, paper [3] used the observation data obtained over the period from 2010 to 2015 at the Geophysical Observatory (GPO) of the Institute of Solar-Terrestrial Physics (ISTP), Siberian branch of Russian Academy of Sciences, in Tory, Buryatia (51°48′ N, 103°04′ E). Mean nightglow (nighttime airglow) was evaluated in spectral ranges of the RGB channels of the color CCD camera for the Eastern Siberia. Paper [4] proposes a system for quick measurement of night sky brightness using CCD camera mosaic images made using a low-cost automated system. Authors of [5] describe all sky imagers used in Las Cumbres astronomic observatory network for automatic evaluation of atmospheric transparency. The obtained cloud maps are used to improve the accuracy of determination of observation conditions. Night sky brightness measurement systems using all sky imagers are described in [6,7]. The findings show that spectral characteristics of light sources shall be considered to ensure accurate astrometric measurements. The effect of various types of natural and man-induced aerosols on the nightglow brightness in the south of Poland was analyzed in [8]. Results show that aerosol particles have significant influence particularly in low light pollution conditions. A procedure for mapping zonal and meridional velocity, mean height and particle sizes of silvery clouds via photometry using identical RGB all sky imagers spaced at 115 km in near-meridional direction is proposed in [9]. Considerable difference was detected in silvery cloud properties in evening and morning twilight. An AOD measurement technique using the RGB all sky imager data is proposed in [10]. The findings show that AOD data obtained via this technique generally correlates with moon photometer data reaching a correlation coefficient higher than 0.9.

The above-mentioned studies are based on using broad-band all sky imagers. The use of all sky imagers with narrow spectral range photo filters is believed to be no less promising for solving such tasks. This allows detecting

almost monochromatic light flux to facilitate and improve the accuracy of atmospheric extinction calculation [11].

In 2021, trial run of the National Heliogeophysical Complex (NHC), RAS, optical instruments [12] was started at GPO ISTP, SB RAS, to carry out monitoring measurements of nightglow in the 400−1650 nm spectral range. This work shows another, besides airglow measurements, application of these instruments. Specifically, a technique is proposed for evaluating atmospheric transparency at dark time using narrow spectral range all sky imager data included in the NHC RAS optical instruments. In addition, the work provides the results of comparison between the obtained atmospheric transparency data and the data obtained from the CIMEL CE-318 sun photometer, included in the AERONET global network of ground-based stations [13], that was placed at GPO ISTP, SB RAS, in 2004−2021. Airglow measurements using narrow-band cameras are currently widely used. Such measurements are performed, for example, within the Meridian Space Weather Monitoring Project supported by the PRC government [14]. Some other research centers are also equipped with such optical instruments. Therefore, the proposed atmospheric transparency evaluation technique may be of interest for many research organizations.

1. Instruments, data and technique

This study uses the data from the KEO Sentry 4 All Sky Imager (hereinafter referred to as ASI0 and ASI1) as part of the Optical Instruments, NHC RAS, designed for detecting spatial distribution of primary emissions from Earth's upper atmosphere. Imager's field of view is 180°, viewing direction is zenith. Spectral range selection is provided by automatically removable interference filters. Cameras have a different set of interference light filters, specifications of which are listed in the table.

Besides narrow-band filters, both imagers have 715−930 nm broadband filters with spectral range blocking with a center at 865 nm and FWHM of 18 nm. Figure 1 shows spectral channels of all sky imagers against the background of the averaged nightglow spectrum in the range of 400−900 nm as of January 23, 2023, measured using the KEO Spectrograph: VISIBLE spectrometer, which is also included in the NHC RAS optical instrument complex. Exposure time for narrow-band channels is—55 s. Exposure time for the OH (715−930 nm) broadband channel is 7 s.

Characteristics of all sky imager filters

№	ASI0		ASI1	
	Center of bandwidth, nm	FWHM, nm	Center of bandwidth, nm	FWHM, nm
1	557.7	2	557.7	2
2	630.0	2	630.0	2
3	840.0	1.8	427.8	2
4	846.5	1.8	589.3	2
5	857.0	1.8	865.0	10

The proposed technique is implemented in three stages. The first stage involves identification of stars in frames. The star recognition and identification technique developed for the KEO Sentinel wide-angle optical system was adapted for the ASI0 and ASI1 imagers [15,16]. Groups of pixels interpreted as stars are being retrieved. Then the azimuth and elevation angle are determined using dependences previously calculated for each retrieved group. Then the time, azimuth and elevation angle of the group of pixels in the frame and of the star from PyEphem were compared [17]. Star intensity in CCD camera ADC counts is calculated at the next stage as follows

$$I = \sum_{0}^{N} I_{np} - N \cdot I_{bckgr}, \tag{1}$$

where N is the number of pixels in the group interpreted as a star; I_{np} are the ADC counts for one pixel in the group; I_{bckgr} is are the mean pixel values in the neighborhood of a star in the ADC counts.

The manufacturer performed absolute calibration for channels with narrow spectral range of the NHC RAS all sky imagers. Data for 557.7 nm and 630 nm spectral channels is hereinafter given in energy units. Total atmospheric optical thickness $\tau(\lambda)_{total}$ is evaluated at the third stage. Calculation is performed for each imager frame and for each identified star, whose exoatmospheric brightnesses are listed in catalogue [18]. The mean number of stars in a frame used for calculation is 9. $\tau(\lambda)_{total}$ for each star is calculated as follows [19]

$$\tau(\lambda)_{total} = \frac{-\ln \frac{E}{E_0}}{M}, \tag{2}$$

where E is the detected brightness of the identified star, E_0 is the exoatmospheric brightness of star for the selected spectral channel [18], M is the optical air mass equal to the zenith angle secant of the star.

Spectral characteristics of stars E_0 were taken from catalogue [18], which provides energy distribution in spectra of 602 stars generated by stars at the top of the Earth's atmosphere. For further analysis, 557.7 nm and 630 nm spectral channels were chosen, that are detected by the NHC RAS all sky imagers with high time resolution and are covered by a spectral range from catalogue [18]. For example, exoatmospheric brightness of Polaris for 577.7 nm and 630 nm, in accordance with the catalogue, are $5.78 \cdot 10{-}2\,\mathrm{erg \cdot cm^{-2} \cdot s^{-1} \cdot cm^{-1}}$ and $5.02 \cdot 10^{-2}\,\mathrm{erg \cdot cm^{-2} \cdot s^{-1} \cdot cm^{-1}}$, respectively. Taking into account the FWHM of 2 nm of the 557.7 nm and 630 nm interference filters, luminosities of the 557.7 nm and 630 nm channels will be equal to $5.78 \cdot 10^{-9}\,\mathrm{erg \cdot cm^{-2} \cdot s^{-1}}$ and $5.02 \cdot 10^{-9}\,\mathrm{erg \cdot cm^{-2} \cdot s^{-1}}$, respectively.

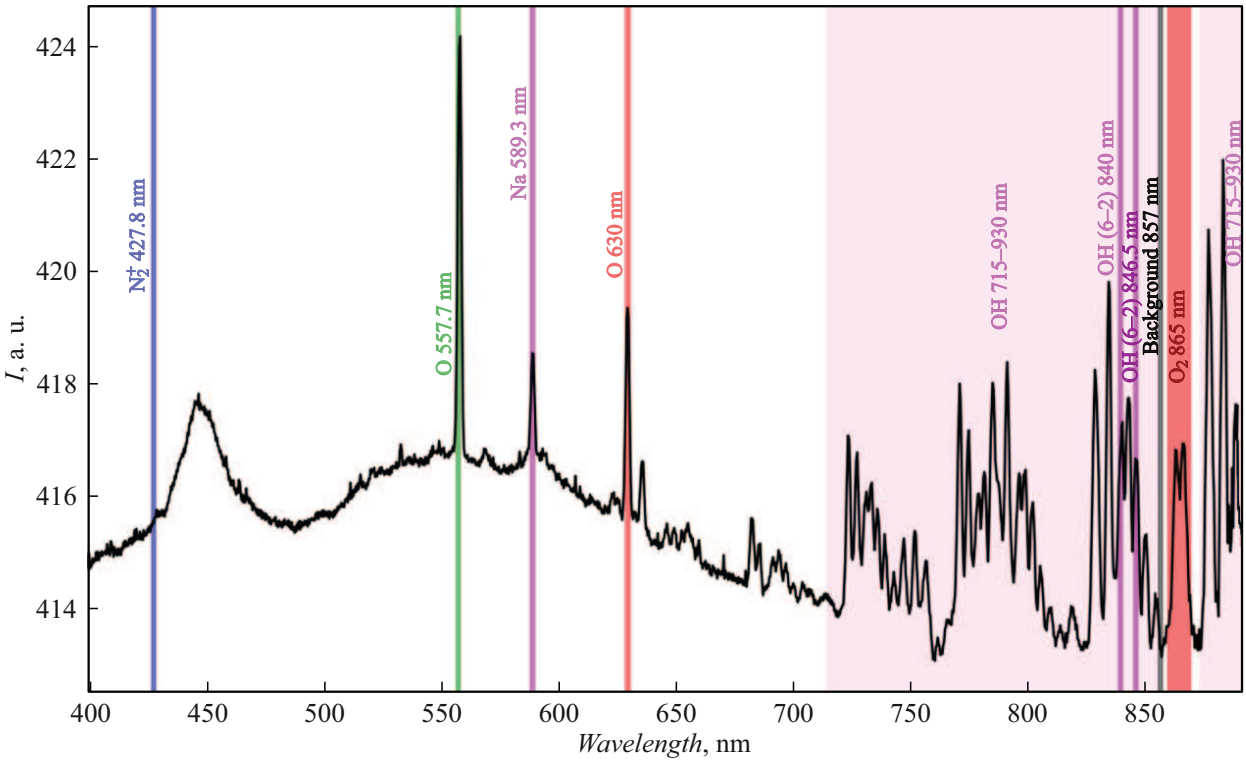

Figure 1. Nightglow spectrum in the range of 400–900 nm (averaged spectrum as of 23.01.2023) measured using the KEO Spectrograph:VISIBLE spectrometer. Spectral channels of the ASI0 and ASI1 all sky imagers are highlighted in color.

For comparison with the data processing results for the ASI0 and ASI1 imagers obtained via the above-mentioned technique, this study uses the total atmospheric optical thickness data obtained using the CIMEL CE-318 automated sun photometer at the GPO ISTP, SB RAS, included in the AERONET global network of ground-based stations [13]. Photometer detects direct solar radiation in 8 spectral channels: 340, 380, 440, 500, 670, 870, 940 and 1020 nm [19]. For comparison, mean daily total atmospheric optical thicknesses at 500 nm and 675 nm from March to November 2021 were used (data processing level 2.0, including cloud filtration [13]). Atmospheric transparency data obtained using the sun photometer at daytime and all sky imager data obtained at nighttime may certainly differ in intraday dynamics, but they shall have common features in reflection of processes on large time scales.

2. Findings and discussion

We had tested the above-mentioned technique for data from the NHC RAS all sky imagers. Figure 2, *a* shows the time variation of the Polaris intensity as of January 1 2022, in 557.7 nm and 630 nm spectral ranges calculated using the above-mentioned technique. Moreover, time variation of intensity averaged in the neighborhood of Polaris in corresponding spectral channels is shown. Figure 2, *b* shows the time variation of the relation between the Polaris intensity detected in the 557.7 nm and 630 nm channels of the ASI0 (E_{star}) imager and the luminosity generated by Polaris at the top of the Earth's atmosphere (E_0) [18]. Results shown in Figure 2 demonstrate the applicability of the technique for interpreting airglow observations. Local maxima at 14:00, 18:30 and 21:40 UT reflect 557.7 nm atmospheric emission variations. Decrease in the calculated intensity of Polaris in the time range of 13–17:30 UT coincides with the mean emission intensity minimum 557.7 nm at 16 UT. This decrease is lower than other minima within the given period, which can be attributed to passage of slight clouds or mist. Decrease in the Polaris intensity by more than three times can be caused by shortcomings of the algorithm of star identification in an imager frame due to image smearing under the action of clouds.

Figure 3 shows a time variation of the intensity of several stars (E_{star}) normalized to their exoatmospheric brightnesses (E_0). Experimental data was obtained using the ASI0 imager on January 01, 2022. Some relative star intensities higher or equal to 1 can be noted (Figure 3, *a*). This can be attributed both to inaccuracies in star catalogue [18] and to star intensity determination algorithm errors. Imagers with narrow light filters have advantages and disadvantages for atmospheric absorption evaluation at dark time. On the one hand, almost monochromatic light flux is detected to facilitate and improve the accuracy of atmospheric extinction calculation [11]. On the other hand, spectral channels of

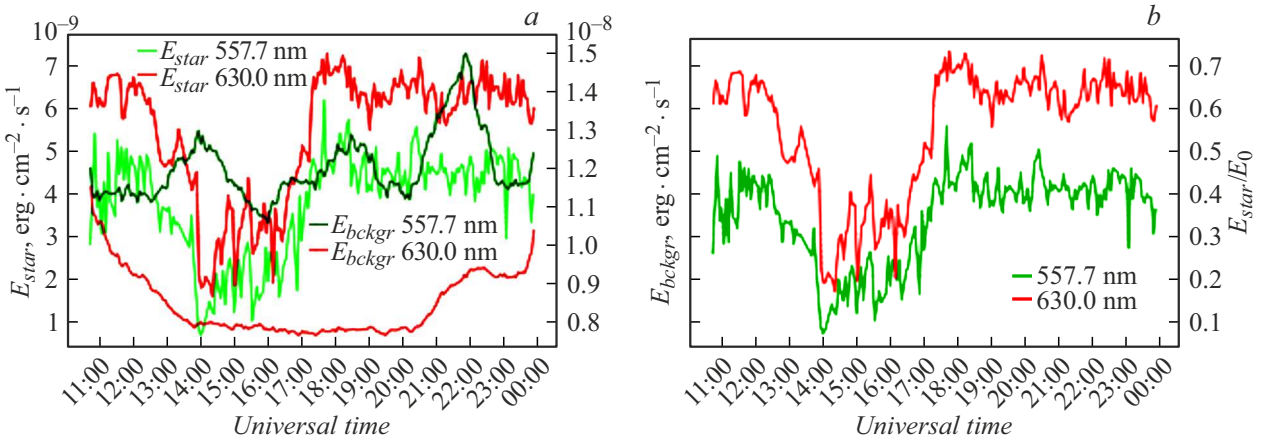

Figure 2. Time variation of the Polaris intensity as of 01.01.2022 calculated from the ASI0 imager data (pane *a*) in 557.7 nm (green curve) and 630 nm (red curve) spectral channels. Dark green and dark red curves — intensity time variation calculated in the neighborhood of Polaris (±5°), in the 557.7 nm and 630 nm spectral channels, respectively. Pane *b* shows the time variation of the times intensity of Polaris normalized to its exoatmospheric brightness in the corresponding spectral ranges [18].

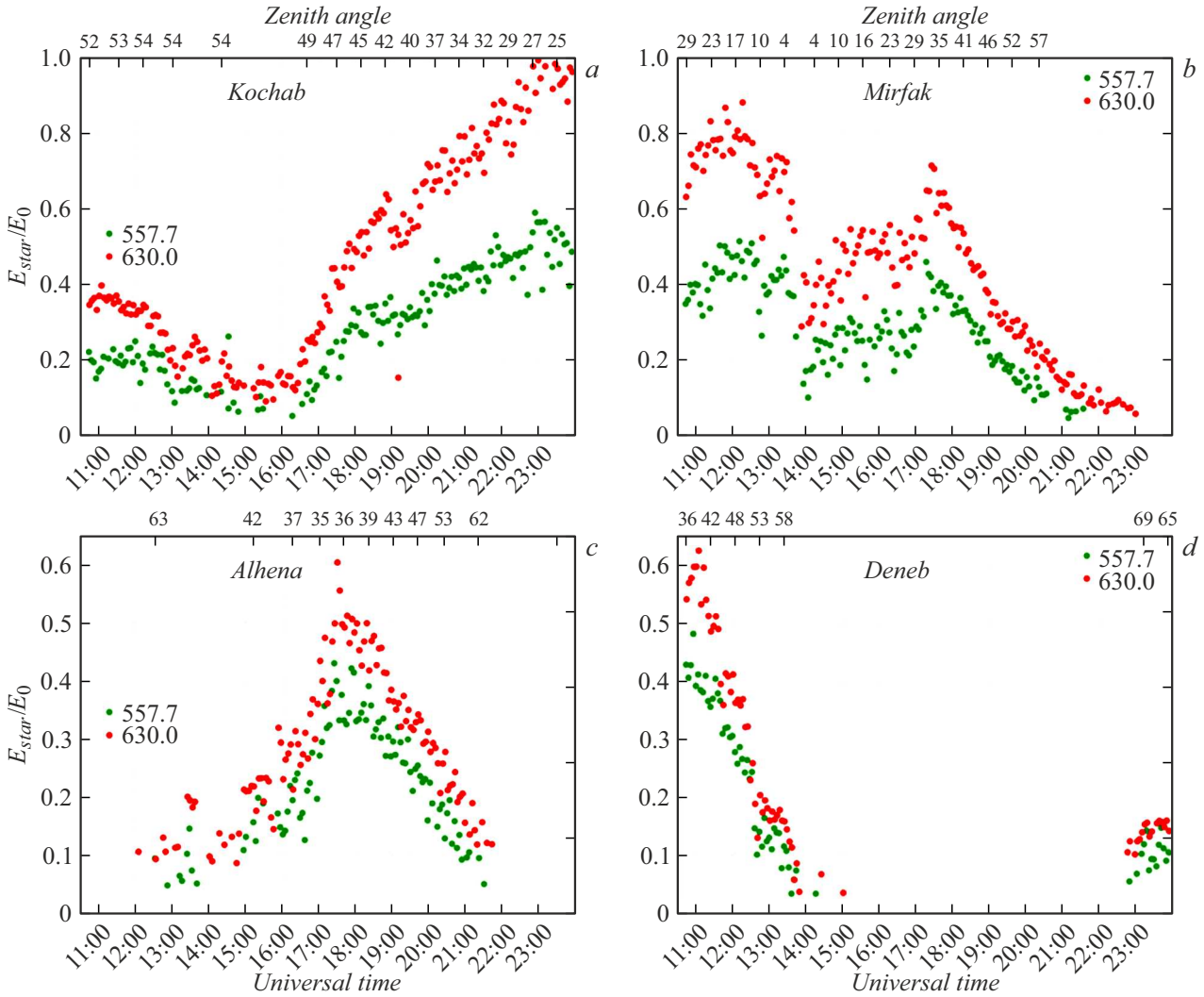

Figure 3. Time variation of the relative intensity of Kochab (*a*), Mirfak (*b*), Alhena (*c*) and Deneb (*d*) as of 01.01.2022 calculated from the ASI0 data in the 557.7 nm (green) and 630 nm (red) spectral channels.

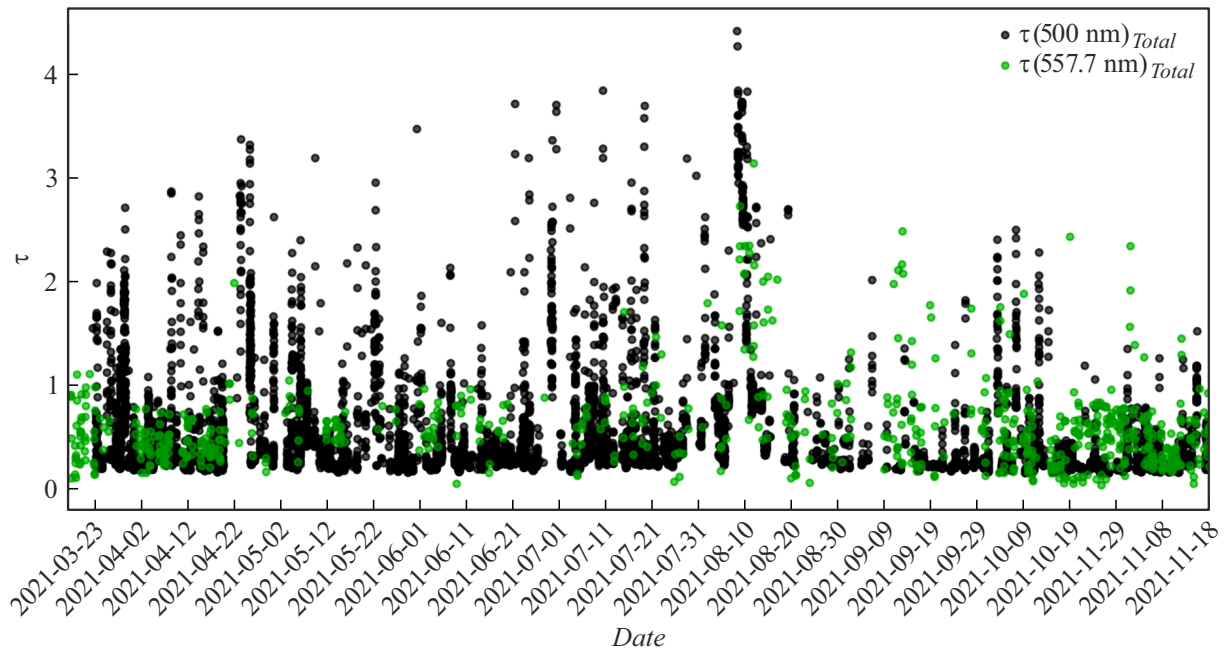

Figure 4. Total atmospheric optical depth for 500 nm according to the CIMEL CE-318 photometer data (black) and 557.7 nm spectral channel data of the all sky imager (green).

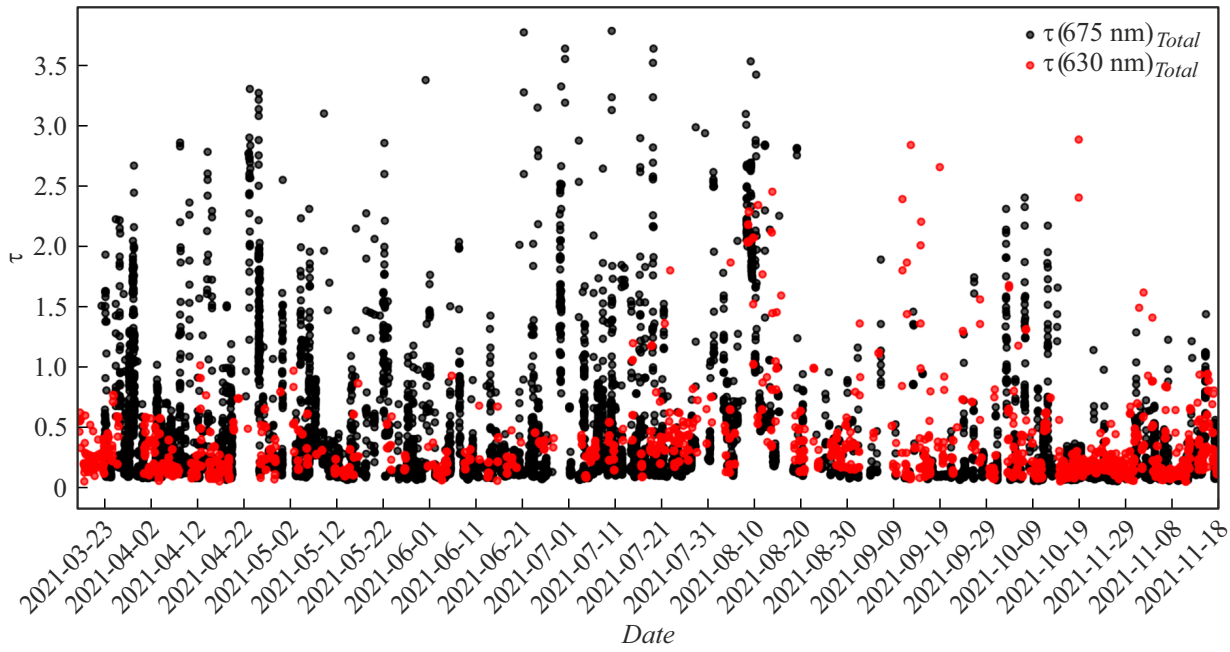

Figure 5. Total atmospheric optical depth for 675 nm according to the CIMEL CE-318 photometer data (black) and 630 nm spectral channel data of the all sky imager (red).

such imagers are set to atmospheric emission glow lines, whose intensities even in geomagnetically quiet nights are comparable with star intensities in a narrow spectral range (Figure 1). This degrades the signal-to-noise ratio in the star identification technique compared with systems with a broad spectral range or a range beyond emission lines or upper atmosphere bands. In addition, imager channels operate in spectral ranges with pronounced absorption, unlike the sun photometer, whose spectral channels were selected taking into account atmospheric transparency windows [20].

In 2021, all sky imagers (at dark time) and the AERONET sun photometer (at daylight time) operated together to allow some kind of comparison. Figures 4 and 5 show total atmospheric optical thickness variations accord-

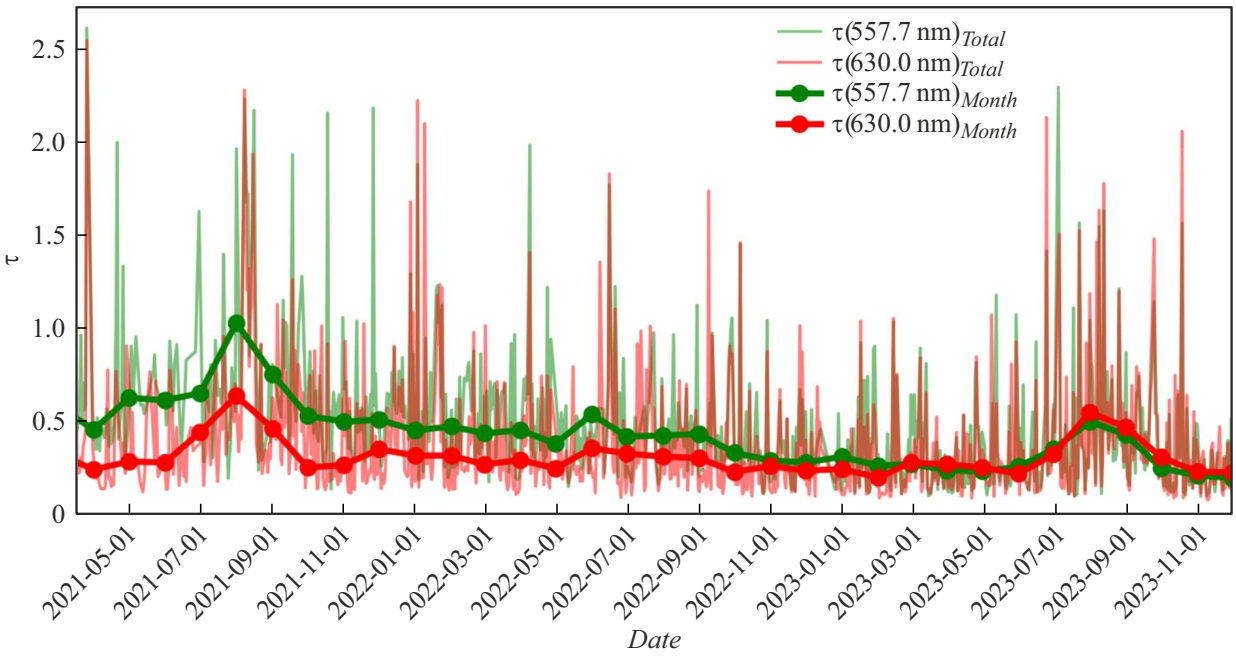

Figure 6. Time variation of daily average (thin lines) and monthly average total atmospheric optical depth according to the NHC all sky imager data in the 557.7 nm (green) and 630 nm (red) spectral lines.

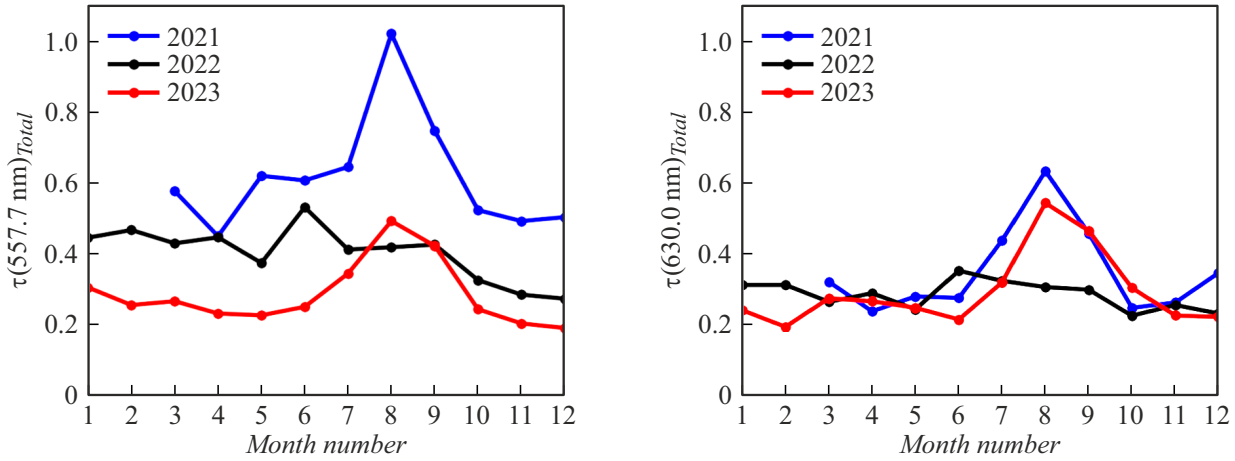

Figure 7. Seasonal variation of the total atmospheric optical depth in 2021–2023 for the 557.7 (left) and 630 nm (right) spectral ranges according to the NHC all sky imager data.

ing to the AERONET photometer data and variations according to the ASI0 all sky imager data during simultaneous operation of these instruments. The closest spectral ranges in the instruments were selected: Figure 4 — 557.7 nm (ASI0) and 500 nm (AERONET), Figure 5 — 630.0 nm (ASI0) and 675 nm (AERONET).

Total atmospheric thicknesses measured by various techniques using the CIMEL photometer in daylight time and the all sky imager at dark time agree quite well with each other (Figure 4, 5). A maximum is identified in August 2021 and is caused by numerous wildfires during this period.

Figure 6 shows the calculated total atmospheric thickness according to the NHC all sky imager data in the 557.7 nm and 630 nm spectral lines for the period from April 2021 to December 2023. Daily average (thin lines) and monthly average (thick lines) values are provided. A slow decreasing trend for total atmospheric optical thicknesses and abrupt decrease in the difference of absorption in the 557.7 nm and 630 nm spectral lines can be seen.

Figure 7 shows a seasonal variation of the total atmospheric thickness for 2021–2023 measured by the NHC all sky imagers. As can be seen from the figure, the total atmospheric thickness maximum for the 557.7 nm and 630 nm spectral ranges is observed in August for 2021 and 2023. In 2022, a typical maximum is not observed. The

smallest total atmospheric thicknesses are observed in spring and autumn months. In [21,22], a yearly average variation of monthly average AOD is provided, reflecting seasonal AOD variations at 380 nm, 500 nm and 870 nm according to the CIMEL CE-318 photometer placed at GPO ISTP, SB RA. It has been found that the largest values of AOD for 380 nm and 500 nm are observed in June, while the largest values of AOD in the 870 nm long-wavelength region fall on August. The total atmospheric thickness variations can generally differ from the AOD variation because, besides the aerosol extinction, the total atmospheric thickness is affected by molecular (Rayleigh) scattering and molecular absorption (water vapor, ozone and other gases).

Conclusion

The findings demonstrate that atmospheric absorption can be evaluated using the data from the narrow-band all sky imager intended for detection of spatial distribution of the Earth's upper atmosphere emission intensity. NHC all sky imagers operate in the monitoring mode and can be used not only in upper atmosphere studies, but also for environmental monitoring and for supplementing the information about lower atmosphere variations. The developed technique fulfils the following tasks: evaluation of atmospheric transparency at dark time; relative calibration of all sky imagers by „reference" clear nights; additional data acquisition for interpreting the data on spatial distribution of atmospheric emission intensity; evaluation of criteria for identification of traveling-wave disturbances (screening of slight clouds, mist, etc.). At this stage, we show that atmospheric transparency can be evaluated according to narrow-band all sky imager data making no claims to measurement accuracy. To increase the technique accuracy, the algorithm for star identification and intensity calculation of stars in a frame shall be improved, and advanced star catalogues and, accordingly, more accurate exoatmospheric star intensity data shall be used. In addition, verification (absolute and relative calibration) of the used all sky imagers is necessary.

Funding

The study was supported financially by the Ministry of Education and Science of the Russian Federation (grant № 075-GZ/C3569/278), experimental data was obtained using the Unique Scientific System UNU „Optical Instruments".

Conflict of interest

The authors declare no conflict of interest.

References

[1] A.V. Mikhalev, M.A. Tashchilin. Optika atmosfery i okeana, **20** (555), 2007 (2016) (in Russian).
[2] A.V. Mikhalev, M.A. Tashchilin, S.M. Sakerin. Optika atmosfery i okeana, **3** (202), 2019 (1995) (in Russian)
[3] A.V. Mikhalev, S.V. Podlesny, P.V. Stoeva. Solnechno-zemnaya fizika, **3** (74), 2016 (2021 (in Russian).
[4] D. Duriscoe, Ch. Luginbuhl, Ch. Moore. Publications of the Astronomical Society of the Pacific, **119** (852), 192 (2007).
[5] N. Volgenau, E. Manne-Nicholas, S. Foale, M. Bowman, D. Harbeck, M. Daily. *Using all-sky cameras tomeasure atmospheric transparency at robotic telescope sites.* In Ch.R. Benn, A. Chrysostomou, L.J. Storrie-Lombardi (editors). *Observatory Operations: Strategies, Processes, and Systems X, volume 13098 of Society of Photo-Optical Instrumentation Engineers (SPIE) Conference Series* (page 130980E, July 2024)
[6] D. Mandat, M. Pech, M. Hrabovsky, P. Schovanek, M. Palatka, P. Travnicek, M. Prouza, J. Ebr. *All Sky Camera instrument for night sky monitoring* (eprint arXiv:1402.4762, 2014)
[7] P. Fiorentin, A. Bertolo, S. Cavazzani, S. Ortolani. Remote Sensing, **15** (17), 4196 (2023).
[8] T. Sciezor, A. Czaplicka. J. Quantitative Spectroscopy and Radiative Transfer, **254**, 107168 (2020).
[9] O.S. Ugolnikov. J. Atmospheric and Solar-Terrestrial Physics, **259**, 106242 (2024).
[10] R. Roman, D. González-Fernández, J.C. Antuna Sánchez, C. Herrero del Barrio, S. Herrero-Anta, Á. Barreto, V.E. Cachorro, L. Doppler, R. González, C. Ritter, D. Mateos, N. Kouremeti, G. Copes, A. Calle, M.J. Granados-Muñoz, C. Toledano, Á.M. de Frutos. Atmospheric Measurement Techniques, **18** (13), 2847 (2025).
[11] W. Romanishin. *An Introduction to Astronomical Photometry Using CCDs* (CreateSpace Independent Publishing Platform, 2014)
[12] R.V. Vasiliev, M.F. Artamonov, A.B. Beletsky, O.S. Zorkaltseva, E.S. Komarova, I.V. Medvedeva, A.V. Mikhalev, S.V. Podlesny, K.G. Ratovsky, T.E. Syrenova, M.A. Tashchilin, I.D. Tkachev. Solnechno-zemnaya fizika, **105** (2020), 72 (2021 (in Russian).
[13] Electronic source. Available at: https://aeronet.gsfc. nasa.gov/ (Date of access: 22.09.2025)
[14] J. Xu, Q. Li, L. Sun, X. Liu, W. Yuan, W. Wang, J. Yue, Sh. Zhang, W. Liu, G. Jiang, K. Wu, H. Gao, Ch. Lai. *The Ground-Based Airglow Imager Network in China* (American Geophysical Union (AGU), 2021), ch. 19, p. 365–394
[15] T.E. Syrenova, A.B. Beletsky, R.V. Vasilyev. Tech. Phys., **67** (15), 2416 (2022). DOI: 10.21883/TP.2022.15.55269.172-21
[16] R.V. Vasilyev, T.E. Syrenova, A.B. Beletsky, M.F. Artamonov, E.G. Merzlyakov, A.V. Podlesny, M.V. Cedric. Atmosphere, **12** (7), 841 (2021).
[17] Electronic source. Brandon Rhodes. PyEphem: Astronomical Computations in Python, 2024 (Date of access: 22.09.2025)
[18] A.V.Kharitonov. *Svodny spektrofotometrichesky katalog zvezd* („Nauka" Kazakhskoy SSR, 1978) (in Russian)
[19] D. Giles, A. Sinyuk, M. Sorokin, J. Schafer, A. Smirnov, I. Slutsker, Th. Eck, B. Holben, J. Lewis, J. Campbell, E. Welton, S. Korkin, A. Lyapustin. Atmospheric Measurement Techniques, **12** (1), 169 (2019).

[20] Electronic source. Available at: https://www.cimel.fr/solutions/ce318-t/ (Date of access: 22.09.2025)
[21] M. Taschilin, A. Mikhalev, D. Kabanov. *Variations of atmospheric aerosol optical depth in the Tunka valley during 2004–2017*. In 24th International Symposium on Atmospheric and Ocean Optics: Atmospheric Physics (SPIE, 2018), v. 10833, p. 108334M.
[22] M. Taschilin, I. Yakovleva, S. Sakerin, O. Zorkaltseva, A. Tatarnikov, E. Scheglova. Atmosphere, **12**, 1706 (2021).

Translated by E.Ilyinskaya